

# Graph Signal Processing over Multilayer Networks – Part II: Useful Tools and Practical Applications

Songyang Zhang, Qinwen Deng, and Zhi Ding, *Fellow, IEEE*

**Abstract**—This work introduces a tensor-based framework of graph signal processing over multilayer networks (M-GSP) to analyze high-dimensional signal interactions. Following Part I’s introduction of fundamental definitions and spectrum properties of M-GSP, this second Part focuses on more detailed discussions of implementation and applications of M-GSP. Specifically, we define the concepts of stationary process, convolution, bandlimited signals, and sampling theory over multilayer networks. We also develop fundamentals of filter design and derive approximated methods of spectrum estimation within the proposed framework. For practical applications, we further present several MLN-based methods for signal processing and data analysis. Our experimental results demonstrate significant performance improvement using our M-GSP framework over traditional signal processing solutions.

**Index Terms**—Multilayer network, graph signal processing, filter design, sampling theory

## I. INTRODUCTION

GRAPH signal processing (GSP) has become an increasingly popular tool for signal processing and data analysis based on graph models [1]. In GSP, signals and their interactions can often be modeled as graph of vertices and edges, respectively [2]. In many broader scenarios, however, a general dataset or system may feature multiple different types of interactions and underlying connections [3]. Inefficient for traditional GSP to process, such more complex systems or datasets can be better described by “multilayer” structures, and modeled by a high-dimensional graph known as multilayer networks [4]. Especially when various layers of the multilayer network represent different inherent natures, treating them as a single-layer equivalent supra-graph [5] is not feasible. On the other hand, different layers are not isolated and should not be modeled by disjoint graphs [6]. To this end, the more general multilayer network represents a suitable graph model for signal analysis and processing. This two-part study presents a tensor-based framework for multilayer network signal processing (M-GSP) and investigates its strengths and limitations.

In Part I [7], we have introduced the theoretical foundation for M-GSP. First, we introduced the tensor representation of multilayer networks, and provided definitions of MLN signals residing on the representing tensor. We described signal shifting over the multilayer network based on tensor contraction. In addition, we provided alternative definitions of spectrum space and singular space of MLN based on tensor factorization [8] and higher-order SVD (HOSVD) [9], respectively, together

with the introduction of the corresponding multilayer network Fourier transform (M-GFT) and singular value transform (M-GST). For interpretability, we provided detailed discussions and some numerical results to illustrate the concept of spectrum and frequency properties. Our theoretical and illustrative results demonstrate that the M-GSP framework can generalize the traditional graph-based GSP and handle “multilayer” interactions in the multilayer networks.

In this second Part II of the series, we examine further the spectrum properties of M-GSP, and explore additional applications. Analogous to the traditional sampling theory, we derive the conditions and properties for perfect signal recovery from samples in M-GSP. We further provide the theoretical foundation for the M-GSP filter designs, spectral convolution, stationary process and spectrum estimation. Additionally, we present several application examples of the proposed M-GSP framework:

- 1) We introduce a signal compression method according to the proposed MLN sampling theory to demonstrate the efficiency and efficacy of M-GSP in describing structured data;
- 2) We develop an image segmentation method according to unsupervised spectrum clustering to illustrate the effect of MLN spectrum analysis.
- 3) We apply MLN convolution in edge detection tasks of multi-color (e.g. RGB) images to demonstrate the practical use of M-GSP in traditional signal processing tasks.
- 4) We introduce a filter-based approach for semi-supervised classification over the multilayer networks.

In various applications, we compare MLN-based methods with traditional GSP-based methods and/or learning algorithms to demonstrate how the proposed M-GSP framework can capture additional “multilayer” features.

We organize the rest of the Part II as follows. Leveraging Part I, we start with a brief overview of the proposed M-GSP in Section II. Next, Section III introduces some efficient tools of M-GSP for data analysis, including filter design, sampling theory, spectral convolution, stationary processes, and spectrum estimation. In Section IV, We provide details on several application examples of M-GSP to demonstrate how it captures the underlying multilayer structure. Lastly, we summarize our works in Section V.

## II. SHORT OVERVIEW OF M-GSP

We briefly review the core concepts of M-GSP from Part I of this two part series [7].

S. Zhang, Q. Deng and Z. Ding are with Department of Electrical and Computer Engineering, University of California, Davis, CA, 95616. (E-mail: sydzhang@ucdavis.edu, mrdeng@ucdavis.edu, and zding@ucdavis.edu).

### A. Multilayer Network and its Tensor Representation

A multilayer network with  $K$  nodes and  $M$  layers is defined as  $\mathcal{M} = \{\mathcal{V}, \mathcal{L}\}$ , where  $\mathcal{V} = \{v_1, v_2, \dots, v_K\}$  is the set of nodes, and  $\mathcal{L} = \{l_1, l_2, \dots, l_M\}$  is the set of layers with each layer  $l_i = \{v_{i_1}, \dots, v_{i_n}\}$  containing a subset of  $\mathcal{V}$ .

Specifically, for a multilayer network  $\mathcal{M}$  with  $|\mathcal{L}| = M$  layers and  $|l_i| = N$  nodes in each layer  $i$ , one can view  $\mathcal{M}$  as  $N$  virtual entities  $\{x_1, \dots, x_N\}$  projected onto  $M$  layers. Then, such a multilayer network  $\mathcal{M}$  can be represented by a fourth-order adjacency tensor  $\mathbf{A} \in \mathbb{R}^M \times \mathbb{R}^N \times \mathbb{R}^M \times \mathbb{R}^N$  defined as

$$\mathbf{A} = (A_{\alpha i \beta j}), \quad 1 \leq \alpha, \beta \leq M, 1 \leq i, j \leq N, \quad (1)$$

where each entry  $A_{\alpha i \beta j}$  of  $\mathbf{A}$  indicates the edge (link) intensity between entity  $j$ 's projection in layer  $\beta$  and entity  $i$ 's projection in layer  $\alpha$  [3]. Generally, we use bold uppercase letters to denote tensors, i.e.,  $\mathbf{A} \in \mathbb{R}^{I_1 \times \dots \times I_N}$  represents an  $N$ th-order tensor with  $I_k$  being the dimension of the  $k$ th order.  $A_{i_1 \dots i_N}$  denotes the entry of  $\mathbf{A}$  in position  $(i_1, i_2, \dots, i_N)$  with  $1 \leq i_k \leq I_k$ . For tensor  $\mathbf{A}_f$  with an index  $f$ , we write its entries as  $[A_f]_{i_1 \dots i_N}$ . In addition to adjacency tensor, Laplacian tensor can be also defined similar to that in normal graphs. Interested reader could refer to Part I [7] for more details.

Although various layers of a general multilayer network may have different numbers of nodes, it is more convenient to normalize them to  $N$  by reconstructing the multilayer networks in one of two different ways:

- For layer  $l_\alpha$  with fewer nodes than  $N$ , add  $N - |l_\alpha|$  isolated (ghost) nodes for the layer to get total nodes.
- For layers with more nodes than  $N$ , aggregate similar nodes to reduce the number of aggregated nodes to  $N$ .

When complexity permits, adding isolated ghost nodes is preferable in practice since their addition does not affect the structure of the layer or the interaction of other connected nodes therein. The second method is sensitive to the aggregation criteria in use.

Flattening is an important tool for analysis by simplifying some tensor operations in M-GSP. For a multilayer network  $\mathcal{M} = \{\mathcal{V}, \mathcal{L}\}$  with  $M$  layers and  $N$  nodes in each layer, its fourth-order representing tensor  $\mathbf{A} \in \mathbb{R}^M \times \mathbb{R}^N \times \mathbb{R}^M \times \mathbb{R}^N$  can be flattened into a second-order matrix in two ways:

- Layer-wise flattening: Tensor  $\mathbf{A}$  can be flattened into a matrix  $\mathbf{A}_{FL} \in \mathbb{R}^{MN} \times \mathbb{R}^{MN}$  via

$$[A_{FL}]_{N(\alpha-1)+i, N(\beta-1)+j} = A_{\alpha i \beta j}. \quad (2)$$

- Entity-wise flattening: Tensor  $\mathbf{A}$  can be flattened into a square matrix  $\mathbf{A}_{FN} \in \mathbb{R}^{NM} \times \mathbb{R}^{NM}$  with element

$$[A_{FN}]_{M(i-1)+\alpha, M(j-1)+\beta} = A_{\alpha i \beta j}. \quad (3)$$

### B. MLN Signals and Signal Shifting

In M-GSP, the signal is defined as a second-order tensor

$$\mathbf{s} = (s_{\alpha i}) \in \mathbb{R}^M \times \mathbb{R}^N, \quad 1 \leq \alpha \leq M, 1 \leq i \leq N, \quad (4)$$

where the entry  $s_{\alpha i}$  is the signal sample attributed in the projected node of entity  $i$  in layer  $\alpha$ . Next, signal shifting is

defined as a contraction between  $\mathbf{A}$  and  $\mathbf{s}$  in one entity-related order and one layer-related order, i.e.,

$$\mathbf{s}' = \mathbf{A} \diamond \mathbf{s} \in \mathbb{R}^M \times \mathbb{R}^N, \quad (5)$$

where  $\diamond$  is the contraction between  $\mathbf{A}$  and  $\mathbf{s}$  in orders 3 and 4, and entries in the shifted signal  $\mathbf{s}'$  are given by

$$s'_{\alpha i} = \sum_{\beta=1}^M \sum_{j=1}^N A_{\alpha i \beta j} s_{\beta j}. \quad (6)$$

### C. Multilayer Network Spectrum Space

Defining a tensor outer product  $\circ$  [8], the representing tensor  $\mathbf{A}$  of an undirected multilayer network can be decomposed into

$$\mathbf{A} \approx \sum_{\alpha=1}^M \sum_{i=1}^N \lambda_{\alpha i} \cdot \mathbf{f}_\alpha \circ \mathbf{e}_i \circ \mathbf{f}_\alpha \circ \mathbf{e}_i \quad (7)$$

where  $\mathbf{f}_\alpha \in \mathbb{R}^M$ ,  $\mathbf{e}_i \in \mathbb{R}^N$  are orthonormal. Through simple redefinitions  $\mathbf{V}_{\alpha i} = \mathbf{f}_\alpha \circ \mathbf{e}_i \in \mathbb{R}^M \times \mathbb{R}^N$  and re-indexing  $\mathbf{V}_{(\alpha-1)N+i} = \mathbf{V}_{\alpha i}$ , we can write

$$\mathbf{A} = \sum_{\alpha=1}^M \sum_{i=1}^N \lambda_{\alpha i} \mathbf{V}_{\alpha i} \circ \mathbf{V}_{\alpha i} = \sum_{k=1}^{MN} \lambda_k \mathbf{V}_k \circ \mathbf{V}_k, \quad (8)$$

Then, the MLN spectral space is defined as the space consisting of all spectral tensors  $\{\mathbf{V}_1, \dots, \mathbf{V}_{MN}\}$ , while the tensor factorization  $\{\mathbf{f}_1, \dots, \mathbf{f}_M\}$  and  $\{\mathbf{e}_1, \dots, \mathbf{e}_N\}$  characterize each layer and entity, respectively.

In addition to the tensor factorization, tensor  $\mathbf{A} \in \mathbb{R}^M \times \mathbb{R}^N \times \mathbb{R}^M \times \mathbb{R}^N$  can be decomposed via HOSVD [9] as

$$\mathbf{A} \approx \mathbf{S} \times_1 \mathbf{U}^{(1)} \times_2 \mathbf{U}^{(2)} \times_3 \mathbf{U}^{(3)} \times_4 \mathbf{U}^{(4)} \quad (9)$$

where  $\times_n$  is the  $n$ -mode product [8] and  $\mathbf{U}^{(n)} = [\mathbf{U}_1^{(n)} \quad \mathbf{U}_2^{(n)} \quad \dots \quad \mathbf{U}_{I_n}^{(n)}]$  is a unitary ( $I_n \times I_n$ ) matrix, with  $I_1 = I_3 = M$  and  $I_2 = I_4 = N$ .  $\mathbf{S}$  is a  $(I_1 \times I_2 \times I_3 \times I_4)$ -tensor of which the subtensor  $\mathbf{S}_{i_n}$  obtained by freezing the  $n$ th index to  $\alpha$ :

- $\langle \mathbf{S}_{i_n=\alpha}, \mathbf{S}_{i_n=\beta} \rangle = 0$  where  $\alpha \neq \beta$ .
- $\|\mathbf{S}_{i_n=1}\| \geq \|\mathbf{S}_{i_n=2}\| \geq \dots \geq \|\mathbf{S}_{i_n=I_n}\| \geq 0$ .

The Frobenius-norms  $\sigma_i^{(n)} = \|\mathbf{S}_{i_n=i}\|$  is the  $n$ -mode singular value, with corresponding singular vectors  $\mathbf{U}^{(i)}$ . Since the representing tensor is symmetric for any 2-dimensions in undirected MLN, there are two modes of singular spectrum, i.e.,  $(\gamma_\alpha, \mathbf{f}_\alpha)$  for mode 1,3, and  $(\sigma_i, \mathbf{e}_i)$  for mode 2,4. More specifically,  $\mathbf{U}^{(1)} = \mathbf{U}^{(3)} = (\mathbf{f}_\alpha)$  and  $\mathbf{U}^{(2)} = \mathbf{U}^{(4)} = (\mathbf{e}_i)$ . Since the joint singular tensor captures consistent information of entities and layers, it can be calculated as

$$(\lambda_{\alpha i}, \mathbf{V}_{\alpha i}) = (\gamma_\alpha \cdot \sigma_i, \mathbf{f}_\alpha \cdot \mathbf{e}_i). \quad (10)$$

Here, we mainly focus on the undirected multilayer networks. For more discussions regarding directed multilayer networks, readers are referred to the Part I of the series [7].

#### D. M-GFT and M-GST

Suppose that  $\mathbf{U}_f = (\mathbf{V}_{\alpha i}) \in \mathbb{R}^M \times \mathbb{R}^N \times \mathbb{R}^M \times \mathbb{R}^N$  consists of the spectral tensors of the representing tensor  $\mathbf{A}$ , where

$$[U_f]_{\alpha i \beta j} = [V_{\alpha i}]_{\beta j}. \quad (11)$$

The M-GFT can be defined as the contraction between  $\mathbf{U}_f$  and the tensor signal  $\mathbf{s} \in \mathbb{R}^M \times \mathbb{R}^N$ , i.e.,

$$\hat{\mathbf{s}} = \mathbf{U}_f \diamond \mathbf{s}. \quad (12)$$

Let  $\mathbf{U}_s = (\mathbf{f}_{\alpha} \circ \mathbf{e}_i) \in \mathbb{R}^M \times \mathbb{R}^N \times \mathbb{R}^M \times \mathbb{R}^N$  consist of the singular vectors of representing tensor  $\mathbf{A}$  in Eq. (9), where

$$[U_s]_{\alpha i \beta j} = [f_{\alpha}]_{\beta} \cdot [e_i]_j. \quad (13)$$

The M-GST can be defined as the contraction between  $\mathbf{U}_s$  and the tensor signal  $\mathbf{s} \in \mathbb{R}^M \times \mathbb{R}^N$ , i.e.,

$$\check{\mathbf{s}} = \mathbf{U}_s \diamond \mathbf{s}. \quad (14)$$

Here we only list the key aspects of M-GFT and M-GST. Interested readers may refer to Part I [7] of the series for further discussions and illustrates on concepts such as layer-wise transform, entity-wise transform and inverse transforms.

### III. TOOLS FOR MULTILAYER NETWORK SIGNAL PROCESSING

Let us introduce several useful tools built within the framework of M-GSP proposed in the Part-I paper [7].

#### A. Filter Design

Filtering is an important tool in signal processing applications such as denoising, feature enhancement, smoothing, and classification. In this section, we introduce an MLN filter design together with its properties based on signal shifting.

1) *Polynomial Filter Design:* Polynomial filters are basic filters in graph signal processing [10], [11]. In M-GSP, first-order filtering consists of basic signal shifting as Eq. (5), i.e.,

$$\mathbf{s}' = f_1(\mathbf{s}) = \mathbf{A} \diamond \mathbf{s}. \quad (15)$$

Similarly, a second order filter can be defined as additional shifting on first-order filtered signal, i.e.,

$$\mathbf{s}'' = f_2(\mathbf{s}) = \mathbf{A} \diamond (\mathbf{A} \diamond \mathbf{s}), \quad (16)$$

whose entries  $s''_{\alpha i}$  are calculated as

$$s''_{\alpha i} = \sum_{\beta=1}^M \sum_{j=1}^N A_{\alpha i \beta j} s'_{\beta j} \quad (17)$$

$$= \sum_{\beta, j} A_{\alpha i \beta j} \sum_{\epsilon, p} A_{\beta j \epsilon p} s_{\epsilon p} \quad (18)$$

$$= \sum_{\epsilon, p} s_{\epsilon p} \sum_{\beta, j} A_{\alpha i \beta j} A_{\beta j \epsilon p} \quad (19)$$

$$= (\mathbf{A} \odot \mathbf{A}) \diamond \mathbf{s}. \quad (20)$$

Here,  $\mathbf{W} = \mathbf{U} \odot \mathbf{V} \in \mathbb{R}^M \times \mathbb{R}^N \times \mathbb{R}^M \times \mathbb{R}^N$  denotes the contraction between two fourth-order tensor  $\mathbf{U}, \mathbf{V} \in \mathbb{R}^M \times \mathbb{R}^N \times \mathbb{R}^M \times \mathbb{R}^N$  in one entity-related order and one layer-related order. Its entries are  $W_{\alpha i \epsilon p} = \sum_{\beta, j} U_{\alpha i \beta j} V_{\beta j \epsilon p}$ .

Let  $\mathbf{A}^{[2]} = \mathbf{A} \odot \mathbf{A}$ . From Eq. (8), we have:

$$A_{\alpha i \beta j}^{[2]} = \sum_{\theta, p} A_{\alpha i \theta p} A_{\theta p \beta j} \quad (21)$$

$$= \sum_{\theta, p} \left( \sum_k \lambda_k [V_k]_{\alpha i} [V_k]_{\theta p} \right) \left( \sum_t \lambda_t [V_t]_{\beta j} [V_t]_{\theta p} \right)$$

$$= \sum_{\theta, p} \left( \sum_{k, t} \lambda_k \lambda_t [V_k]_{\alpha i} [V_k]_{\theta p} [V_t]_{\beta j} [V_t]_{\theta p} \right)$$

$$= \sum_{k, t} \lambda_k \lambda_t [V_k]_{\alpha i} [V_t]_{\beta j} \left( \sum_{\theta, p} [V_t]_{\theta p} [V_k]_{\theta p} \right)$$

$$= \sum_{k, t} \lambda_k \lambda_t [V_k]_{\alpha i} [V_t]_{\beta j} \langle \mathbf{V}_k, \mathbf{V}_t \rangle$$

$$= \sum_k \lambda_k^2 [V_k]_{\alpha i} [V_k]_{\beta j}, \quad (22)$$

where  $\langle \cdot, \cdot \rangle$  denotes the inner product.

Similarly, for  $\tau$ th-order term  $\mathbf{A}^{[\tau]}$ , its entry  $A_{\alpha i \beta j}^{[\tau]}$  can be calculated as

$$A_{\alpha i \beta j}^{[\tau]} = \sum_k \lambda_k^\tau [V_k]_{\alpha i} [V_k]_{\beta j}. \quad (23)$$

Now we have the following property.

**Property 1.** *The  $\tau$ -th order basic shifting filter  $f_\tau(\mathbf{s})$  can be calculated as*

$$f_\tau(\mathbf{s}) = \mathbf{A}^{[\tau]} \diamond \mathbf{s} \quad (24)$$

$$= \left( \sum_{k=1}^{MN} \lambda_k^\tau \mathbf{V}_k \circ \mathbf{V}_k \right) \diamond \mathbf{s}. \quad (25)$$

This property is the M-GSP counterpart to the traditional linear system interpretation that complex exponential signals are eigenfunction of linear systems [2], [12], and provides a quicker implementation of higher-order shifting. With the  $k$ -order polynomial term, the adaptive polynomial filter can be defined as

$$h(\mathbf{s}) = \sum_k \alpha_k \mathbf{A}^{[k]} \diamond \mathbf{s}, \quad (26)$$

where  $\{\alpha_k\}$  are parameters to be estimated from data.

Adaptive polynomial filter is useful in semi-supervised classification [12], [13] and exploits underlying geometric topologies. We will illustrate further and provide application examples based on MLN polynomial filtering in Section IV.

2) *Filter Design Optimization:* Filters designed through optimization based on geometric information play an important role in semi-supervised signal processing works, such as classification, denoising, and prediction [11]–[17]. We can also design filters based on similar optimization approaches. Let an MLN optimization-based filter be denoted by  $\mathbf{s}' = f(\mathbf{s}, \mathbf{A})$  where  $\mathbf{s}$  is the input signal. The filter design for  $f(\cdot)$  can be posed as an optimization formulation:

$$\min_f F_1(\mathbf{s}, \mathbf{s}') + \sigma F_2(\mathbf{s}', \mathbf{A}). \quad (27)$$

Here,  $F_1$  denotes a chosen empirical loss, such as the least square loss or the hinge loss, whereas  $F_2$  is a regularization loss, such as Laplacian regularization and total variation. In addition to optimization when designing filter  $f(\cdot)$ , some applications focus on optimization of the filtered signal  $\mathbf{s}'$

directly, which manifests a similar form as the traditional graph-based semi-supervised learning approaches [18].

### B. Multilayer Network Spectral Convolution

Graph-based spectral convolution is effective in applications such as feature extraction, classification, and in design of graph convolutional networks [19], [20]. Graph convolution can be implemented indirectly in the transform domain [21]:

$$\mathbf{x} \star \mathbf{y} = \mathcal{F}^{-1}(\mathcal{F}(\mathbf{x}) * \mathcal{F}(\mathbf{y})), \quad (28)$$

where  $*$  is the element-wise Hadamard product,  $\mathcal{F}$  is the graph Fourier transform (GFT) and  $\mathcal{F}^{-1}$  represents inverse GFT. This formulation exploits the property that graph convolution in vertex domain is equivalent to spectrum domain product.

In [22], a more general definition of graph convolution take the filtering form, i.e.,

$$\mathbf{x} \star \mathbf{y} = f(\mathbf{x}) = (GFT^{-1} \text{diag}(\hat{\mathbf{y}}) GFT) \cdot \mathbf{x}, \quad (29)$$

where  $GFT^{-1}$  consists of eigenvectors of the representing matrix as columns and  $\hat{\mathbf{y}}$  can be interpreted as filter parameters in graph spectrum domain. Note that, Eq. (28) and Eq. (29) have the same mathematical formulation. For convenience, we define spectral convolution over MLN in a similar mathematical formulation as follows.

**Definition 1** (MLN Spectral Convolution). *In M-GSP, the spectral convolution is calculated as*

$$\mathbf{x} \star \mathbf{y} = \mathcal{F}_{MLN}^{-1}(\mathcal{F}_{MLN}(\mathbf{x}) * \mathcal{F}_{MLN}(\mathbf{y})), \quad (30)$$

where  $\mathcal{F}_{MLN}$  is the M-GFT and  $\mathcal{F}_{MLN}^{-1}$  is the inverse M-GFT [7]. Then, the MLN convolutional filter with parameters  $\mathbf{c}$  on the signal  $\mathbf{s}$  is defined by

$$f_{\mathbf{c}}(\mathbf{s}) = \mathbf{c} \star \mathbf{s}. \quad (31)$$

In view of traditional DSP and GSP, MLN spectral convolution focuses on multilayer geometric features. We shall provide application examples of MLN convolution in Section IV to demonstrate the strength of M-GSP over traditional GSP and DSP in exemplary signal processing tasks.

### C. Stationary Processes over Multilayer Network

Graph stationarity is the key conception, which allows GSP to more easily analyze certain random signal types and multiple observations of nodes over graphs [23]. Moreover, authors of [24], [25] relied on graph stationary process to propose methods to estimate spectrum and diffusion for multiple observations of nodes over graphs. In this part, we propose a stationary process definition with the MLN framework.

From definition of the polynomial filter in Eq. (24), strict-sense stationary process can be defined as follows.

**Definition 2** (Strict-Sense Stationary Process). *A stochastic signal  $\mathbf{x} \in \mathbb{R}^M \times \mathbb{R}^N$  is strict-sense stationary over the multilayer network with representing tensor  $\mathbf{A}$  if and only if*

$$\mathbf{x} \stackrel{d}{=} \mathbf{A}^{[\tau]} \diamond \mathbf{x} \quad (32)$$

holds for any  $\tau$ .

Since strict-sense stationarity is difficult to verify and analyze for real-life datasets, we are interested in weak-sense stationarity over MLN similar to that in DSP and GSP [23].

**Definition 3** (Weak-Sense Stationary Process). *A stochastic signal  $\mathbf{x} \in \mathbb{R}^M \times \mathbb{R}^N$  is weak-sense stationary over the multilayer network with representing tensor  $\mathbf{A}$  if and only if*

$$\mathbb{E}[\mathbf{x}] = \mathbb{E}[\mathbf{A}^{[\tau]} \diamond \mathbf{x}], \quad (33)$$

$$\mathbb{E}[(\mathbf{A}^{[\tau_1]} \diamond \mathbf{x})(\mathbf{A}^{[-\tau_2]} \diamond \mathbf{x})^H] = \mathbb{E}[(\mathbf{A}^{[\tau_1+\tau_2]} \diamond \mathbf{x})(\mathbf{A}^{[\tau-\tau_2]} \diamond \mathbf{x})^H] \quad (34)$$

both hold for any integers  $\tau$ ,  $\tau_1$ , and  $\tau_2$ .

Eq. (33) implies that the mean function of signals must be constant for the MLN stationary process. In Eq. (34),  $\mathbf{A}^{[-\tau]}$  could be interpreted as the propagation in the reverse direction of  $\mathbf{A}$ . Thus, Eq. (34) indicates that the signal covariance function only depends on the difference of time steps, i.e.,  $\tau_1 + \tau_2$ , which is consistent with classic signal processing [26].

Similar to GSP, we can also relate spectrum tensor to covariance matrix of signals. Recall that representing tensors can be flattened as Eq. (2) and Eq. (3), and corresponding signals can be flattened as follows:

- Layer-wise flattening:  $\mathbf{s}_L \in \mathbb{R}^{MN}$  with entries:

$$[\mathbf{s}_L]_{N(\alpha-1)+i} = s_{\alpha i}. \quad (35)$$

- Entity-wise flattening:  $\mathbf{s}_N \in \mathbb{R}^{NM}$  with entries:

$$[\mathbf{s}_N]_{M(i-1)+\alpha} = s_{\alpha i}. \quad (36)$$

Recall from our Part I paper [7] that these two flattening methods would lead to the same eigenvalues, whereas their eigenvectors are simply reshaped eigen-tensors. Suppose that  $\mathbf{A}_F$  is one of the flattened tensor and  $\mathbf{s}_F$  is the correspondingly flattened signal. The flattened polynomial filter can be calculated as

$$\mathbf{s}'_F = \mathbf{A}_F^T \mathbf{s}_F. \quad (37)$$

Since the inverse propagation can be represented as  $\mathbf{A}_F^H$ , we have the following property:

**Property 2.** *A stochastic signal  $\mathbf{x}$  is weak-sense stationary if and only if its flattened signal  $\mathbf{x}_F$  has zero-mean and its covariance matrix has the same eigenvectors as the flattened spectral tensors, i.e.,*

$$\mathbb{E}[\mathbf{x}_F] = \mathbf{0}, \quad (38)$$

$$\mathbb{E}[\mathbf{x}_F \mathbf{x}_F^H] = \mathbf{V}_F \Sigma_{\mathbf{x}} \mathbf{V}_F^H, \quad (39)$$

where  $\Sigma_{\mathbf{x}}$  is diagonal,  $\mathbf{V}_F$  contains all the flattened spectral tensors as its columns, and  $(\cdot)^H$  is the Hermitian transpose.

*Proof.* Here we show the proof of Property 2.

*Mean Function:* Since  $\mathbf{A}_F$  is symmetric here for undirected multilayer networks,

$$\mathbf{A}_F^{\tau} = \underbrace{\mathbf{V}_F \Lambda \mathbf{V}_F^H \cdots \mathbf{V}_F \Lambda \mathbf{V}_F^H}_{\tau \text{ times}} \quad (40)$$

$$= \mathbf{V}_F \Lambda^{\tau} \mathbf{V}_F^H. \quad (41)$$

Then, Eq. (38) can be written as

$$\mathbb{E}[\mathbf{x}_F] = \mathbf{V}_F \Lambda^{\tau} \mathbf{V}_F^T \mathbb{E}[\mathbf{x}_F]. \quad (42)$$

Since  $\mathbf{V}_F \Lambda^\tau \mathbf{V}_F^H$  is not identity for general MLN, Eq. (38) holds for arbitrary MLN if and only if  $\mathbb{E}[\mathbf{x}_F] = \mathbf{0}$ .

*Covariance Function:* Substituting decomposition of  $\mathbf{A}_F$  into its flattened representation of Eq. (34), i.e.,

$$\mathbb{E}[(\mathbf{A}_F^{\tau_1} \mathbf{x}_F)((\mathbf{A}_F^H)^{\tau_2} \mathbf{x}_F)^H] = \mathbb{E}[(\mathbf{A}_F^{\tau_1+\tau_2} \mathbf{x}_F)((\mathbf{A}_F^H)^{\tau_2-\tau_1} \mathbf{x}_F)^H],$$

we have

$$\mathbf{A}_F^{\tau_1} \mathbb{E}[\mathbf{x}_F \mathbf{x}_F^H] \mathbf{A}_F^{\tau_2} = \mathbf{A}_F^{\tau_1+\tau_2} \mathbb{E}[\mathbf{x}_F \mathbf{x}_F^H] \mathbf{A}_F^{\tau_2-\tau_1}. \quad (43)$$

Then we obtain

$$\begin{aligned} & \mathbf{V}_F \Lambda^{\tau_1} \mathbf{V}_F^H \mathbb{E}[\mathbf{x}_F \mathbf{x}_F^H] \mathbf{V}_F \Lambda^{\tau_2} \mathbf{V}_F^H \\ &= \mathbf{V}_F \Lambda^{\tau_1+\tau_2} \mathbf{V}_F^H \mathbb{E}[\mathbf{x}_F \mathbf{x}_F^H] \mathbf{V}_F \Lambda^{\tau_2-\tau_1} \mathbf{V}_F^H \end{aligned} \quad (44)$$

Multiplying  $[\mathbf{V}_F \Lambda^{\tau_1}]^{-1}$  to the left and  $[\mathbf{V}_F^H]^{-1} \Lambda^{\tau-\tau_2}$  to the right for both sides of Eq.(44), we have

$$\Lambda^\tau \mathbf{V}_F^H \mathbb{E}[\mathbf{x}_F \mathbf{x}_F^H] \mathbf{V}_F = \mathbf{V}_F^H \mathbb{E}[\mathbf{x}_F \mathbf{x}_F^H] \mathbf{V}_F \Lambda^\tau. \quad (45)$$

For Eq. (45) to hold for general MLN,  $\mathbf{V}_F^H \mathbb{E}[\mathbf{x}_F \mathbf{x}_F^H] \mathbf{V}_F$  should be diagonal, i.e.,

$$\mathbf{V}_F^H \mathbb{E}[\mathbf{x}_F \mathbf{x}_F^H] \mathbf{V}_F = \Sigma_{\mathbf{x}}, \quad (46)$$

which completes the proof of Eq. (39).  $\square$

#### D. Direct Spectrum Estimation over MLN

In practical applications, systems or datasets do not readily provide an explicit MLN structure in advance. Forming an MLN would often require estimation of distances among nodes and can be time-consuming. Fortunately, we can bypass such complexity and estimate MLN spectrum directly from datasets based on signal properties, e.g., smoothness or stationarity [27]–[30]. In this part, we mainly focus on two scenarios:

- **Multiple Observations of Nodes:** We first focus on cases involving multiple observations for each node, where  $\mathbf{x} \in \mathbb{R}^M \times \mathbb{R}^N \times \mathbb{R}^t$ . Here,  $M$  is the number of layers,  $N$  is the number of nodes in each layer and  $t$  is the number of observations. Obviously, we could flatten the signal into  $\mathbf{x}_F \in \mathbb{R}^{MN} \times \mathbb{R}^t$ . Assuming that the signal follows the stationary process, we can estimate the spectrum based on the Property 2 according Algorithm 1.

---

#### Algorithm 1 Spectrum Estimation based on Stationary Process

---

- 1: **Input:** Signals  $\mathbf{x} \in \mathbb{R}^M \times \mathbb{R}^N \times \mathbb{R}^t$ ;
  - 2: Flatten the third-order signal into  $\mathbf{x}_F \in \mathbb{R}^{MN} \times \mathbb{R}^t$ ;
  - 3: Find the row-wise mean  $\bar{\mathbf{x}}_F$  of  $\mathbf{x}_F$  and normalize  $\mathbf{x}_F$  as zero-mean, i.e.,  $\mathbf{x}'_F = \mathbf{x}_F - \bar{\mathbf{x}}_F \cdot \mathbf{1}$  with  $\mathbf{1} \in \mathbb{R}^{1 \times t}$ ;
  - 4: Decompose  $\mathbf{x}'_F \mathbf{x}'_F{}^H$  to obtain the flattened spectrum  $\mathbf{V}_F \in \mathbb{R}^{MN} \times \mathbb{R}^{MN}$  and reshape it as  $\mathbf{U} \in \mathbb{R}^M \times \mathbb{R}^N \times \mathbb{R}^M \times \mathbb{R}^N$ ;
  - 5: **Output:** Spectrum  $\mathbf{U}$ .
- 

- **General Single-Observation Signal:** In a more typical setup, there is only one set of observations for  $MN$  nodes. A multilayer network with  $M$  layers and  $N$  nodes in each layer can be viewed as  $M$  projections of  $N$  virtual entities onto  $M$  layers. Here, we propose a PCA-style method to estimate the layer-wise spectrum and

entity-wise spectrum as outlined in Algorithm 2. Different from Algorithm 1 focusing on the stationarity of multiple observations, Algorithm 2 provides two structural perspectives of multilayer networks. Interested readers may refer to our Part I paper [7] for more details of flattening and network structure. Later, we shall also compare the performance of applying the two estimation algorithms with decomposition for some application examples in Section IV.

---

#### Algorithm 2 Spectrum Estimation for 1D Signals

---

- 1: **Input:** Signals  $\mathbf{x} \in \mathbb{R}^M \times \mathbb{R}^N$ ;
  - 2: Normalize  $\mathbf{x}$  as column-wise zero mean and calculate the eigenvectors  $\mathbf{E} = \{\mathbf{e}_1, \dots, \mathbf{e}_N\}$  of the covariance matrix  $\mathbf{x}^H \mathbf{x} \in \mathbb{R}^N \times \mathbb{R}^N$ ;
  - 3: Normalize  $\mathbf{x}$  as row-wise zero mean and calculate the eigenvectors  $\mathbf{F} = \{\mathbf{f}_1, \dots, \mathbf{f}_M\}$  of the covariance matrix  $\mathbf{x} \mathbf{x}^H \in \mathbb{R}^M \times \mathbb{R}^M$ ;
  - 4: Calculate the spectral tensor  $\mathbf{U} = \{\mathbf{f}_\alpha \circ \mathbf{e}_i\}$ ;
  - 5: **Output:** Spectrum  $\mathbf{U} \in \mathbb{R}^M \times \mathbb{R}^N \times \mathbb{R}^M \times \mathbb{R}^N$
- 

#### E. Sampling Theory

Sampling attempts to find a selected set of important nodes to fully or approximately capture the full features of the entire population [31]. In GSP, sampling theory [22], [32]–[34] attracted attentions owing to some successes in compression and storage. In this section, we discuss the sampling of MLN graph signals.

1) *Sampling in Vertex Domain:* In the M-GSP framework, sampling aims to select a subset of signals to describe some global information. Generally there are three paths to reduce signal sizes: 1) reducing number of layers; 2) reducing number of entities; and 3) reducing number of nodes. To better interpret MLN sampling, we start with sampling of tensor signals. In Part I [7], we introduced an  $n$ -mode product  $\times_n$  to modify the dimension of specific orders [8]. It is intuitive to apply the  $n$ -mode product also to define sampling and interpolation operations here.

**Definition 4** (Block-wise Sampling and Interpolation). *Consider the sampling of a signal  $\mathbf{s} \in \mathbb{R}^M \times \mathbb{R}^N$  over MLN into  $P$  layers with index  $\{p_1, p_2, \dots, p_P\}$  and  $Q$  entities with index  $\{q_1, q_2, \dots, q_Q\}$ . The sampling operation is defined by*

$$\mathbf{s}_D = \mathbf{s} \times_1 \mathbf{S}_P \times_2 \mathbf{S}_Q \in \mathbb{R}^P \times \mathbb{R}^Q \quad (47)$$

where sampling operator  $\mathbf{S}_P \in \mathbb{R}^P \times \mathbb{R}^M$  consists of elements

$$[S_P]_{ij} = \begin{cases} 1 & j = p_i \\ 0 & \text{otherwise} \end{cases}, \quad (48)$$

and  $\mathbf{S}_Q \in \mathbb{R}^Q \times \mathbb{R}^N$  with elements calculated as

$$[S_Q]_{ij} = \begin{cases} 1 & j = q_i \\ 0 & \text{otherwise} \end{cases}. \quad (49)$$

The interpolation operation is defined as

$$\mathbf{s}_R = \mathbf{s}_D \times_1 \mathbf{T}_M \times_2 \mathbf{T}_N \in \mathbb{R}^M \times \mathbb{R}^N, \quad (50)$$

where  $\mathbf{T}_M \in \mathbb{R}^M \times \mathbb{R}^P$  and  $\mathbf{T}_N \in \mathbb{R}^N \times \mathbb{R}^Q$ .

Let us examine the steps in Eq. (47). Let  $\mathbf{w} = \mathbf{s} \times_1 \mathbf{S}_P$ . From the definition of  $n$ -mode product [8], entries of  $\mathbf{w}$  are

$$w_{ij} = \sum_{k=1}^M s_{kj} \cdot [S_P]_{ik}, \quad (51)$$

which indicates that

$$\mathbf{w} = \mathbf{S}_P \cdot \mathbf{s} \in \mathbb{R}^P \times \mathbb{R}^N. \quad (52)$$

Let  $\mathbf{v} = \mathbf{w} \times_2 \mathbf{S}_Q$ . We have

$$v_{ij} = \sum_{k=1}^N w_{ik} \cdot [S_Q]_{jk}, \quad (53)$$

which implies  $\mathbf{v} = \mathbf{w} \cdot \mathbf{S}_Q^T$ . Now, we have the following property to calculate the sampled signal.

**Property 3.** *With sampling operators  $\mathbf{S}_P \in \mathbb{R}^P \times \mathbb{R}^M$  and  $\mathbf{S}_Q \in \mathbb{R}^Q \times \mathbb{R}^N$ , the sampled signal can be calculated as*

$$\mathbf{s}_D = \mathbf{S}_P \cdot \mathbf{s} \cdot \mathbf{S}_Q^T. \quad (54)$$

Moreover, if sampling is in a specific order, i.e., entity-wise or layer-wise, we have the following definitions.

**Definition 5** (Order-wise Sampling and Interpolation). *Given signal  $\mathbf{s} \in \mathbb{R}^M \times \mathbb{R}^N$  which is to be downsampled into  $P$  layers, the layer-wise sampling is defined as*

$$\mathbf{s}_{LD} = \mathbf{S}_P \cdot \mathbf{s} \in \mathbb{R}^P \times \mathbb{R}^N, \quad (55)$$

and the interpolation operation is defined as

$$\mathbf{s}_{LR} = \mathbf{T}_M \cdot \mathbf{s}_{LD} \in \mathbb{R}^M \times \mathbb{R}^N, \quad (56)$$

with  $\mathbf{S}_P \in \mathbb{R}^P \times \mathbb{R}^M$  and  $\mathbf{T}_M \in \mathbb{R}^M \times \mathbb{R}^P$ . Moreover, if the signal is to be sampled into  $Q$  entities, then entity-wise sampling is defined by

$$\mathbf{s}_{ND} = (\mathbf{S}_Q \cdot \mathbf{s}^T)^T \in \mathbb{R}^M \times \mathbb{R}^Q, \quad (57)$$

and the interpolation operation is defined as

$$\mathbf{s}_{NR} = (\mathbf{T}_N \cdot \mathbf{s}_{ND}^T)^T \in \mathbb{R}^M \times \mathbb{R}^N \quad (58)$$

with  $\mathbf{S}_Q \in \mathbb{R}^Q \times \mathbb{R}^N$  and  $\mathbf{T}_N \in \mathbb{R}^N \times \mathbb{R}^Q$ .

In addition to Definition 4, we also define node-wise down-sampling based on the flattened signal as follows.

**Definition 6** (Node-wise Sampling based on Flattening Analysis). *Suppose that  $\mathbf{s}_F \in \mathbb{R}^{MN \times 1}$  is the flattened signal to be downsampled into  $K$  nodes, whose indices are  $\{v_1, v_2, \dots, v_K\}$ , sampling is defined by*

$$\mathbf{s}_{FD} = \mathbf{S}_F \cdot \mathbf{s}_F \in \mathbb{R}^{K \times 1}, \quad (59)$$

where the sampling operator  $\mathbf{S}_F \in \mathbb{R}^K \times \mathbb{R}^{MN}$  is defined by

$$[S_F]_{ij} = \begin{cases} 1 & j = v_i \\ 0 & \text{otherwise} \end{cases}. \quad (60)$$

Interpolation is defined by

$$\mathbf{s}_{FR} = \mathbf{T}_F \cdot \mathbf{s}_{FD} \in \mathbb{R}^{MN \times 1}, \quad (61)$$

where  $\mathbf{T}_F \in \mathbb{R}^{MN} \times \mathbb{R}^K$ .

The node-wise sampling here follows the same definition as in basic GSP sampling [32] by flattening MLN into a supra-graph. Naturally for MLN with a single layer, entity-wise and block-wise sampling also reduce to basic GSP sampling operations. Still, for applications where different layers cannot be treated equivalently for the  $N$  entities, M-GSP sampling is more general and can be more efficient, to be further illustrated in Section IV-D.

Different sampling operations in M-GSP can target different applications. For example, if we want to sample several data points with multiple features, we can model the dataset as a multiplex network where each layer represents one feature and can implement entity-wise sampling to select key data points to target specific purposes. For another example, for tasks involving layer aggregation or reduction such as the reduction of video frames, layer-wise sampling is quite suitable. On the other hand, for tasks involving reduction of total number of nodes with a regularized structure such as sampling pixels in an RGB image, block-wise sampling operation is well suited.

Given the definitions of sampling operations, we next analyze conditions under which original signals may be fully recovered from the sampled signals. To derive such *recovery conditions*, we first define bandlimited signals.

**Definition 7** (Bandlimited Signal). *Suppose that  $\hat{\mathbf{s}} = \mathcal{F}(\mathbf{s}) \in \mathbb{R}^M \times \mathbb{R}^N$  is  $M$ -GST or  $M$ -GFT of the original signal  $\mathbf{s} \in \mathbb{R}^M \times \mathbb{R}^N$ . Signal  $\hat{\mathbf{s}}$  is said to be  $(K, T)$ -bandlimited if*

$$\hat{s}_{\alpha i} = 0, \quad \alpha \geq K, \quad i \geq T. \quad (62)$$

Moreover, the signal is  $K$  flat-bandlimited if its flattened transformation signal  $\hat{\mathbf{s}}_F \in \mathbb{R}^{MN}$  have

$$[\hat{s}_F]_i = 0, \quad i \geq K. \quad (63)$$

Here, bandlimited signals are not necessarily ordered by eigenvalues or singular values to describe low-pass or smoothness as discussed in [32]. The order of spectrum here limits the number of non-zero supports. Since the ordering of spectrum is not specified, we can rearrange the eigenvalues and reshape the transformed signal tensor. Such generalization is potentially useful to represent non-smooth graph signals. Specifically, if we only focus on sampling ratio, we could reshape the flattened signal into

$$\hat{\mathbf{s}}_F = \begin{bmatrix} \hat{\mathbf{s}}_{FK} \\ \mathbf{0}_{MN-K} \end{bmatrix}, \quad (64)$$

where  $\hat{\mathbf{s}}_{FK} \in \mathbb{R}^{K \times 1}$  consists of all nonzero elements as support. We can reshape the tensor signal as

$$\hat{\mathbf{s}} = \begin{bmatrix} \hat{\mathbf{s}}_{K,T} & \mathbf{0}_{M,N-T} \\ \mathbf{0}_{M-K,T} & \mathbf{0}_{M-K,N-T} \end{bmatrix}, \quad (65)$$

where  $\hat{\mathbf{s}}_{K,T}$  contains as few zeros as possible.

In addition, if we sort eigenvalues and/or singular values in descending order, the bandlimited signal is low-pass in top-left block of its tensors, and is smooth in the first part for the flattened signal. To summarize, bandlimited signals have the following recovery property:

**Property 4.** *For a  $K$ -bandlimited flattened signal  $\mathbf{s}_F$ , full recovery from  $Z$  samples is achievable if  $Z \geq K$ .*

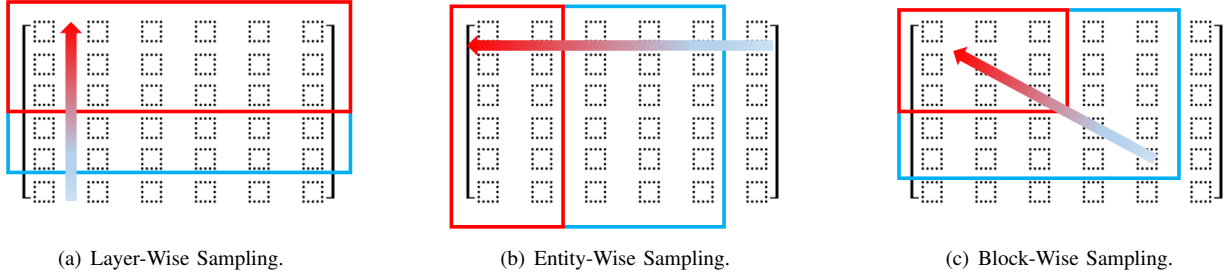


Fig. 1. Options of Sampling Directions for Tensor Signals.

Since the flattened signal has a similar form as in GSP, it shares a similar conclusion on full recovery. For proof of Property 4 and selection of interpolation operators, interested readers may refer to [32] for more details. This property indicates that full recovery is possible for signals with a few non-zero elements in the MLN spectrum domain of known supports. For tensor signals, we also have the following property.

**Property 5.** For a  $(K, T)$ -bandlimited signal  $\mathbf{s}$ , full recovery is available if it is sampled into  $P$  layers and  $Q$  entities such that  $P \geq K$  and  $Q \geq T$ .

Since the  $(K, T)$ -bandlimited tensor signal can be flattened into a vector-wise  $Z$ -bandlimited signal with  $KT \geq Z$ , it is straightforward to prove Property 5 from Property 4. The tensor-based sampling theory could be useful for applications that need to reduce the number of entities, layers, and nodes from datasets with structure limitations as mentioned before.

---

**Algorithm 3** Sampling of Tensor Signal in Spectral Domain

---

- 1: **Input:** Signals  $\mathbf{s} \in \mathbb{R}^M \times \mathbb{R}^N$ ;
  - 2: Transform the signal into spectral space as  $\hat{\mathbf{s}} \in \mathbb{R}^M \times \mathbb{R}^N$  via M-GFT or M-GST;
  - 3: Reorder the elements in  $\hat{\mathbf{s}}$  via certain rules;
  - 4: Sample the transformed signal in the left top as  $\hat{\mathbf{s}}_D \in \mathbb{R}^P \times \mathbb{R}^Q$ ;
  - 5: Interpolate zeros in the right bottom of  $\hat{\mathbf{s}}_D$  as  $\hat{\mathbf{s}}_R \in \mathbb{R}^M \times \mathbb{R}^N$ ;
  - 6: Implement the inverse MLN transform on  $\hat{\mathbf{s}}_R$  to obtain the recovered signal  $\mathbf{s}_R \in \mathbb{R}^M \times \mathbb{R}^N$ .
  - 7: **Output:** Sampled coefficients  $\hat{\mathbf{s}}_D$  and recovered signal  $\mathbf{s}_R$ .
- 

2) *Sampling in Spectral Domain:* Beyond direct sampling in the vertex domain, it can be more convenient and straightforward to sample signals in spectrum domain. By ignoring the zeros in spectrum domain, we can easily recover the full signal from samples by adding zeros back to sampled signal transforms before taking the inverse transform. Sampling in spectrum domain is intuitive for the lossless sampling and recovery. Here we shall focus on the lossy sampling of tensor-based signals. Generally, we can sample signals in spectrum domain according to Algorithm 3. We reshape transformed signals in terms of eigenvalues or transformed values from top left to bottom right in descending order. When sampling a sub-block in  $\hat{\mathbf{s}}$ , there are three different directions shown

in Fig. 1. Depending on the structure and features of the underlying dataset, different methods may be suitable for different tasks. We will show examples of data compression based on the MLN sampling theory in Section IV-D.

#### IV. APPLICATION EXAMPLES

We now provide some illustrative application examples by considering different proposed tools within our M-GSP framework.

##### A. Image Segmentation

Image segmentation is widely applied in computer vision with various applications such as target sensing, object detection, texture recognition, and compression [35]. Compared with supervised segmentation which generally focuses on classification of pixels, unsupervised segmentation is used to deliver more general labels, such as “foreground” and “background”, in scenarios that require image/video interpretation without prior knowledge. Among various unsupervised methods, spectral clustering is a direct and important method. Spectral clustering groups data points in graph spectral domain. Moreover, spectral clustering is simple to implement by using basic algebraic software. In fact, the result of spectral clustering itself may be a useful metric to evaluate the quality of the spectrum definition. In this part, we introduce an MLN spectral clustering for unsupervised RGB image segmentation.

To model an RGB image using MLN, we can directly treat the three colors as three layers. To reduce the number of nodes for computational efficiency, we first build 1000 superpixels for a given image and represent each superpixel as an entity in the multilayer network, as shown in Fig. 3(b). Here, we define the feature of a superpixel by the mean of all pixels therein. For interlayer connections, each node connects with its counterparts in other layers. For intralayer connections in layer  $\ell$ , we calculate the Gaussian-based distance between two superpixels according to

$$W_{ij} = \begin{cases} \exp\left(-\frac{|\mathbf{s}_i(\ell) - \mathbf{s}_j(\ell)|^2}{\delta_\ell^2}\right), & |\mathbf{s}_i(\ell) - \mathbf{s}_j(\ell)|^2 \leq t_\ell; \\ 0, & \text{otherwise,} \end{cases} \quad (66)$$

where  $\mathbf{s}_i(\ell)$  is the superpixel value in layer  $\ell$ ,  $\delta_\ell$  is an adjustable parameter and  $t_\ell$  is a predefined threshold. Different layers may have different structures. The threshold  $t$  is set to

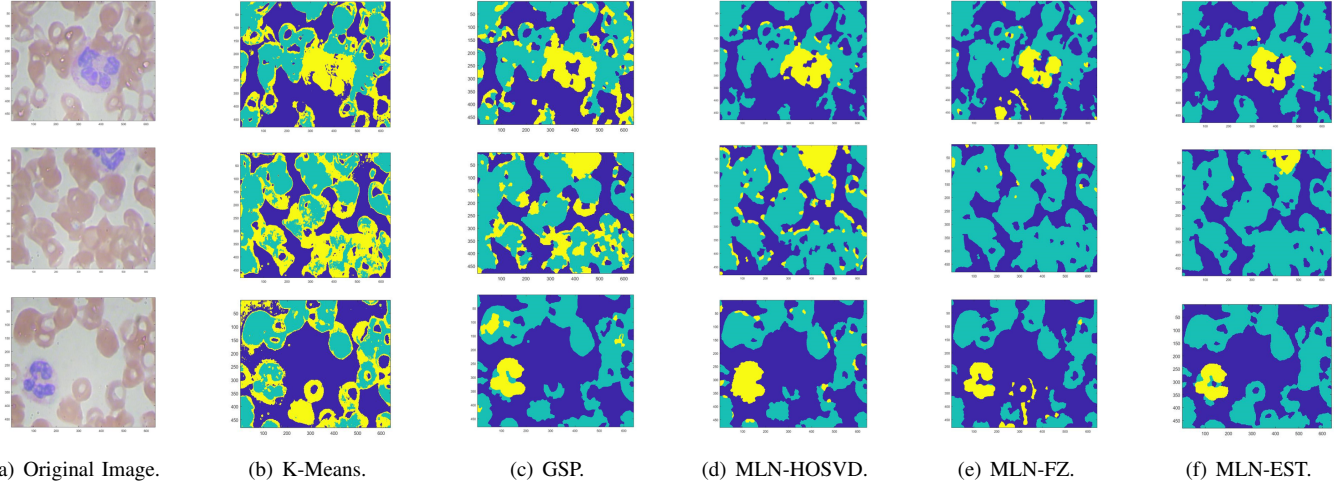


Fig. 2. Example Results of BCCD Image Segmentation.

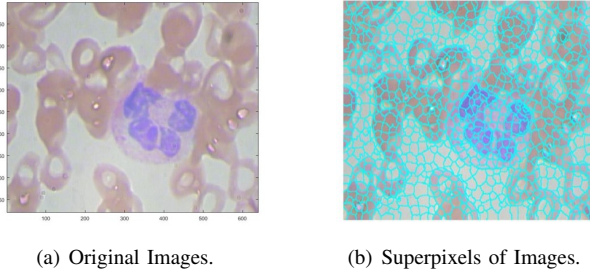


Fig. 3. Example of Datasets.

---

**Algorithm 4** MLN-based Spectral Clustering for Image Segmentation

---

- 1: **Input:** RGB Image  $\mathbf{I} \in \mathbb{R}^P \times \mathbb{R}^Q \times \mathbb{R}^3$ ;
  - 2: Build 1000 superpixels for the image  $\mathbf{I}$  and calculate the value of superpixel based on the mean of all pixels inside that superpixel, i.e.,  $\mathbf{s} \in \mathbb{R}^{1000} \times \mathbb{R}^3$ ;
  - 3: Construct a multilayer network  $\mathbf{A} \in \mathbb{R}^M \times \mathbb{R}^N \times \mathbb{R}^M \times \mathbb{R}^N$  with  $M = 3$  and  $N = 1000$ ;
  - 4: Find the entity-wise spectrum  $\mathbf{E} = [\mathbf{e}_1, \dots, \mathbf{e}_N] \in \mathbb{R}^N \times \mathbb{R}^N$ ;
  - 5: Select the first  $K$  important leading spectrum based on the eigenvalues (singular values) of  $\mathbf{E}$  as  $\mathbf{C} \in \mathbb{R}^N \times \mathbb{R}^K$ ;
  - 6: Cluster each row of  $\mathbf{C}$ , and assign the  $i$ th superpixel into  $j$ th cluster if the  $i$ th row of  $\mathbf{C}$  is clustered into  $j$ th group;
  - 7: Assign all pixels inside one superpixel to the cluster of that superpixel;
  - 8: **Output:** The segmented image.
- 

be the mean of all pairwise distances. As such, an RGB image is modeled as 3-layer multiplex network with  $N = 1000$  nodes.

We then introduce MLN-based spectral clustering. For image segmentation, we focus on the properties of entities (i.e., superpixels), and implement spectral clustering over entity-wise spectrum using Algorithm 4. In Step 4, different schemes

may be used to calculate spectrum, including spectral vector via tensor factorization in Eq. (7), singular vector via HOSVD in Eq. (9), and spectrum estimation via Algorithm 2. In Step 5,  $K$  is determined based on the largest arithmetic gap in eigenvalues. Traditional clustering methods, such as  $k$ -means clustering [37], can be carried out in Step 6.

To test the proposed algorithm, we first compare its results with those from GSP-based method and traditional  $k$ -means clustering by using a public BCCD blood cell dataset shown in Fig. 3(a) ([https://github.com/Shenggan/BCCD\\_Dataset](https://github.com/Shenggan/BCCD_Dataset)). In this dataset, there are mainly three types of objects, i.e., White Blood Cell (WBC) vs. Red Blood Cell (RBC) vs. Platelet (P). We set the number of clusters to 3. For GSP-based spectral clustering, we construct graphs based on the Gaussian model Eq. (66) by using information from all 3 color values  $\sum_{\ell=1}^3 |\mathbf{s}_i(\ell) - \mathbf{s}_j(\ell)|^2$  to form edge connections in a single graph. There is only a single  $\delta_\ell$  and  $t_\ell$  in the Gaussian model.

For M-GSP, we use the MLN singular vectors (MLN-HOSVD), tensor factorization (MLN-FZ) and estimation given in Algorithm 2 (MLN-EST) for spectrum clustering, separately. Their respective results for 3 different images are shown in Fig 2. The WBCs are marked yellow, and the RBCs are marked green. The Platelet (P) is marked blue. From the illustrative results, we can see that graph-based methods perform better than traditional  $k$ -means clustering implemented directly on RGB images. Head-to-head against GSP-based method, MLN methods exhibit better robustness and are better in detecting regions under noise. For example, for the first and second images, GSP-based method is less reliable on a number of boundary areas whereas MLN methods are more accurate when compared against the ground truth from Fig. 2(a).

Comparing results from different MLN-based methods, we find MLN-FZ to be less stable than HOSVD, partly due to approximation algorithms used for tensor factorization. Overall, MLN-EST shows reliable and robust performance over GSP-based method and  $k$ -means.

In addition to visual inspection of results for such im-

TABLE I  
RESULTS OF IMAGE SEGMENTATION IN IMAGE BSD300 AND BSD500

	BSD300(N=100)	BSD300(N=300)	BSD300(N=100, Coarse)	BSD300(N=300, Coarse)	BSD300(N=900,Carse)	BSD500(Corase)
GSP	0.1237	0.1149	0.3225	0.3087	0.3067	0.3554
K-MEANS	0.1293	0.1252	0.3044	0.3105	0.3124	0.3154
MLN-HOSVD	0.1326	<b>0.1366</b>	0.3344	0.3394	0.3335	<b>0.3743</b>
MLN-CP	0.1321	0.1293	0.3195	0.3256	0.3243	0.3641
MLN-EST	<b>0.1376</b>	<u>0.1317</u>	<b>0.3769</b>	<b>0.3611</b>	<b>0.3554</b>	0.3727
IIC						0.2071
GS						0.3658
BP						0.3239
DFC						<u>0.3739</u>

ages, we are further interested to numerically evaluate the performance of the proposed methods against some state-of-art methods for several more complex datasets that contain more classes. For this purpose, we test our methods on the BSD300 and BSD500 datasets [38]. BSD300 contains 300 images with labels, and BSD500 contains 500 images with labels. We first cluster each image, and label each cluster with the best map of cluster orders against the ground truth. Numerically, we use mIOU (mean of Intersection-over-Union), also known as the mean Jaccard Distance, for all clusters in each image to measure the performance. The Jaccard Distance between two groups  $A$  and  $B$  is defined as follows:

$$J(A, B) = \frac{|A \cap B|}{|A \cup B|}. \quad (67)$$

A larger mIOU indicates stronger performance. To better illustrate the results, we considered two setups of datasets, i.e., one containing fewer classes (coarse) and one containing all images (all). We compare our methods together with  $k$ -means, GSP-based spectral clustering, invariant information clustering (IIC) [39], graph-based segmentation (GS) [40], back propagation (BP) [41] and differentiable feature clustering (DFC) [35] in Table I. The best performance is marked in bold whereas the second best value is underlined.

From the results of Table I, we can see that larger number clusters of the first two columns generate worse performance. There are two natural reasons. First, the mapping of best order of cluster labels is more difficult for more classes. Second, the graph-based spectral clustering is sensitive to the number of  $K$  leading spectra and the structure of graphs. It is harder to build a optimal graph and determine the number of  $K$  for larger number of clusters. Regardless, MLN-based methods still provide better performance. Moreover, even we use the same total number of nodes in a single layer graph and multilayer network for fair comparison in terms of complexity, i.e.,  $N = 300$  for graph and  $N = 100$  for MLN, MLN-based methods still perform better than graph-based methods. For the coarse scenarios with fewer clusters, geometry-based methods generally work better. MLN methods have competitive performances compared to the state-of-art methods. Note that, under proper training, neural network (NN)-based methods may give good results in cases with many clusters as suggested in [35]. For this reason, future works may consider graph-based or MLN-based neural networks in image segmentation.

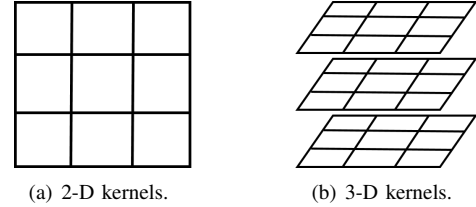


Fig. 4. Example of Convolution Kernels.

### B. Edge Detection

Convolution-based method has been widely used for edge detection of images. Defining a patch-wise window block kernel in convolution, sharp features or high-frequency components can be extracted from images. Similarly, we can also develop edge detection methods based on the MLN convolution:

$$\mathbf{s}' = f_c(\mathbf{s}) = \mathbf{c} \star \mathbf{s}, \quad (68)$$

where  $\mathbf{c}$  is a defined kernel.

In traditional processing, one can first transfer RGB to gray-scale images for edge detection using operators such as Prewitt, Canny and Sobel [42], [43]. Similar to GSP and hypergraph signal processing (HGSP), graph convolution methods could also detect edges in gray-scale images [19]. Unlike traditional (graph) signal processing, M-GSP can model RGB images by using 3-D windows/blocks and define 3-D convolution kernels as shown in Fig. 4(b). Note that, by reshaping each 2-D image frame into a vector for all 3 layers, we also reshape the 3-D M-GSP kernels into a 2-D matrix  $\mathbf{c} \in \mathbb{R}^3 \times \mathbb{R}^N$  accordingly to work with 2-D image signals  $\mathbf{s} \in \mathbb{R}^3 \times \mathbb{R}^N$ . Note that  $N$  denotes the number of pixels in each frame, e.g.,  $N = 9$  in Fig. 4(b). Similarly, the 2-D GSP kernel works with a 1-D signal  $\mathbf{s}_G \in \mathbb{R}^K$  with  $K = 9$  in Fig. 4(a).

To construct an MLN for edge detection, we also represent each of the 3 RGB color by a layer and connect each pixel in one layer with its counterparts in other layers for interlayer connections. The major difference in MLN construction that differs from that for image segmentation lies in the intralayer connections. Here, each pixel is connected with its four adjacency neighbors for intralayer connections. The benefit of constructing such graph is to bypass the computation needed to regenerate spectrum for each window (block), since such graph structure applies to all blocks with the same size.

In general, one can first extract smooth image features, before applying edge detection on the difference between

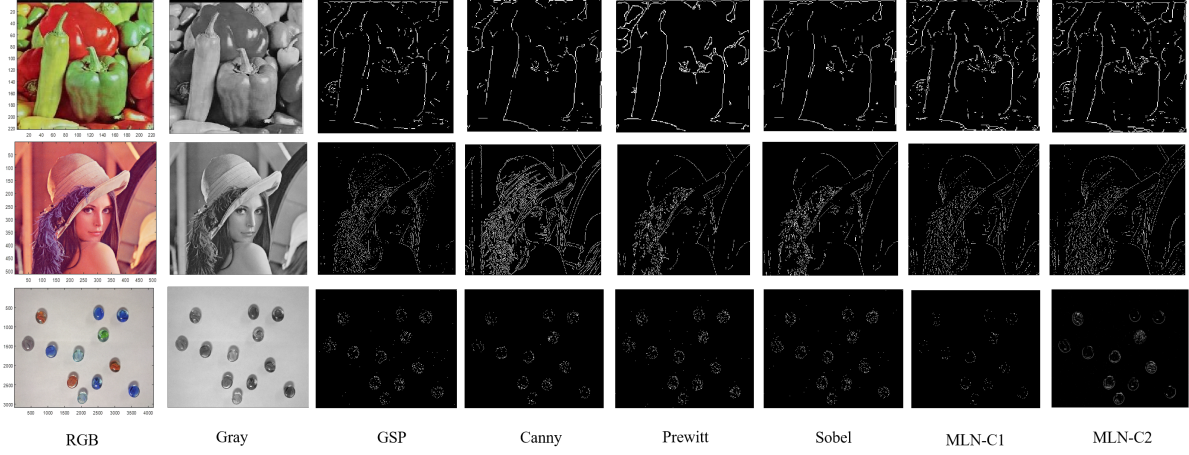


Fig. 5. Results of Edge Detection.

original and smoothed images. To define a graph localization kernel for smoothing, we start from the single-layer graph. Define a graph convolution kernel as follows:  $\mathbf{c} \in \mathbb{R}^K$

$$[c]_i = \begin{cases} 1, & i = k_1, k_2, \dots, k_z, \text{ where } z \leq K; \\ 0, & \text{otherwise,} \end{cases} \quad (69)$$

The convolution output for a signal  $\mathbf{s} \in \mathbb{R}^K$  is simply

$$\begin{aligned} \mathbf{s}' &= \mathbf{V}[(\mathbf{V}^T \mathbf{s}) * (\mathbf{V}^T \mathbf{c})] \\ &= [\mathbf{f}_1, \dots, \mathbf{f}_K] \cdot \left( \begin{bmatrix} \mathbf{f}_1^T \mathbf{s} \\ \vdots \\ \mathbf{f}_K^T \mathbf{s} \end{bmatrix} * \begin{bmatrix} \sum_i [f_1]_{k_i} \\ \vdots \\ \sum_i [f_K]_{k_i} \end{bmatrix} \right) \\ &= \sum_j (\mathbf{f}_j \mathbf{f}_j^T \mathbf{s} \sum_i [f_j]_{k_i}), \end{aligned} \quad (71)$$

where  $\mathbf{V} = [\mathbf{f}_1, \dots, \mathbf{f}_K]$  is the graph spectrum and  $*$  denotes Hadamard product. Different from a pure shift, Eq. (71) enhances information around nodes  $\{v_{k_i}\}$ . With locally-enhanced gray-scale images, we can replace the centroid value of the window (block) by the mean of the convolution outputs inside that window to smooth signals further. By shifting the window over the entire image, one can obtain a locally-enhanced blurred gray-scale image. Since we aim to smooth signals within the window, we can simply localize the information around the center of the block. Here, we define a MLN kernel  $\mathbf{c}_1 \in \mathbb{R}^3 \times \mathbb{R}^N$  with entries

$$[c_1]_{pq} = \begin{cases} 1, & p = 2, q = (N^2 + 1)/2; \\ 0, & \text{otherwise,} \end{cases} \quad (72)$$

to smooth the signal around the center node of the entire network, and define another  $\mathbf{c}_2 \in \mathbb{R}^3 \times \mathbb{R}^N$  with entries

$$[c_2]_{pq} = \begin{cases} 1, & p = 1, 2, 3, \text{ and } q = (N^2 + 1)/2; \\ 0, & \text{otherwise,} \end{cases} \quad (73)$$

to smooth the signal around the center of each of the 3 layers. The M-GSP convolution process is described in Steps 4-6 of Algorithm 5. Whereas convolution can smooth images, one way of edge detection is by examining the explicit difference between the smoothed image and its original, as specified

in Algorithm 5. Usually, parameter  $\tau$  may be set closer to zero to detect edges. In Step 3, we apply the eigen-tensor decomposition instead of singular tensor as sharper edges are closely related to high-frequency components as defined in [7]. The MLN edge detection results can be visually examined in Fig. 5, together with results from several classic detection methods (e.g., Canny, Prewitt, Sobel) and a GSP-based method from [21]. Compared to the traditional methods, MLN-based methods yield more smooth edges and with clearer details, especially for the images with peppers and marbles. From visual inspection, the proposed methods detect the edges with better efficacy in these results.

---

#### Algorithm 5 MLN-based Edge Detection

---

- 1: **Input:** RGB Image  $\mathbf{I} \in \mathbb{R}^P \times \mathbb{R}^Q \times \mathbb{R}^3$ ;
  - 2: Define a 3-D kernel  $\mathbf{c} \in \mathbb{R}^k \times \mathbb{R}^k \times \mathbb{R}^3$  with  $k \leq P, Q$ , and reshape it to  $\mathbf{c}_i \in \mathbb{R}^3 \times \mathbb{R}^N$  with  $N = k^2$ ;
  - 3: Construct a multilayer network with  $M = 3$  layers and  $N$  nodes in each layers and calculate its eigen-tensors;
  - 4: Define a window block of the image  $\mathbf{I}_W \in \mathbb{R}^k \times \mathbb{R}^k \times \mathbb{R}^3$  and reshape it to the MLN signal  $\mathbf{s}_W \in \mathbb{R}^3 \times \mathbb{R}^N$ ;
  - 5: Implement the MLN convolution between  $\mathbf{c}_i$  and  $\mathbf{s}_W$  to obtain the convolved signal  $\mathbf{s}'_W = \mathbf{c}_i * \mathbf{s}_W$ ;
  - 6: Calculate the entity-wise mean of  $\mathbf{s}'_W$  as  $\bar{\mathbf{s}}_W \in \mathbb{R}^{3 \times 1}$  and make it as the new value of the center pixel;
  - 7: Move the window over the whole image and repeat Step 4-6 to calculate the new values of all pixels;
  - 8: Find the gray-scale image of the convolved results and find its differences from the original gray-scale image of the RGB ones;
  - 9: Set a threshold  $\tau$  for the differences to detect edges;
  - 10: **Output:** The detected edges.
- 

### C. Semi-Supervised Classification

Semi-supervised classification is an important practical application for graph-based signal processing. In this part, we

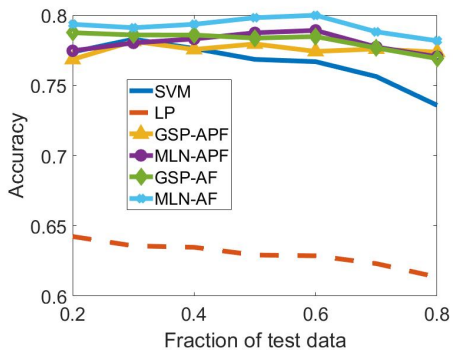


Fig. 6. Results of Classification.

apply MLN polynomial filters for semi-supervised classification. Traditional GSP defines adaptive filter [11] as

$$f(\mathbf{s}) = \sum_i a_i \mathbf{W}^i \mathbf{s}, \quad (74)$$

where  $\mathbf{W}$  is an adjacency matrix based on pairwise distance as described in Eq. (66) or a representing matrix constructed from the adjacency matrix. Here, signals are defined as labels or confidence values of nodes:

$$\mathbf{s} = \begin{bmatrix} \mathbf{s}_L \\ \mathbf{0}_{UL} \end{bmatrix}, \quad (75)$$

by setting unlabeled signals to zero. Optimization can be formulated for specific support to estimate parameters  $a_i$  of  $f(\cdot)$ , e.g., the mean square error (MSE) from ground truth label  $\mathbf{y}_L$

$$\min_{\mathbf{a}} \|\mathbf{M}(f(\mathbf{s}))_L - \mathbf{y}_L\|_2^2, \quad (76)$$

where  $\mathbf{M}(\cdot)$  is a mapping of filtered signals to their discrete labels. For example, in a  $\{\pm 1\}$  binary classification, one can assign a label to a filtered signal against a threshold (e.g. 0). Some other objective functions include labeling uncertainty, Laplacian regularization, and total variation. Using estimated parameters, we can filter the signal once again to determine labels for some unlabeled data by following the same process. The idea of such iterative filtering is similar to that of label propagation [44], in which the labels converge after sufficient iterations of propagation.

Similarly, in an MLN, we can also apply polynomial filters for label estimation. Given an arbitrary dataset  $\mathbf{X} = [\mathbf{x}_1, \dots, \mathbf{x}_N] \in \mathbb{R}^K \times \mathbb{R}^N$  with  $N$  nodes and  $K$  features for each node, we can construct a multilayer network with  $M = K$  layers and  $N$  nodes in each layer. For interlayer connections, each node connects with its counterparts in other layers. For intralayer connections, we define distance between two nodes according to Eq. (66) for each layer. Let its adjacency tensor  $\mathbf{A} \in \mathbb{R}^M \times \mathbb{R}^N \times \mathbb{R}^M \times \mathbb{R}^N$ . A signal is defined by

$$\mathbf{s} = \begin{bmatrix} \mathbf{s}_L & \cdots & \mathbf{s}_L \\ \mathbf{0}_{UL} & \cdots & \mathbf{0}_{UL} \end{bmatrix}^T \in \mathbb{R}^{M \times N}, \quad (77)$$

which is an extended version of Eq. (75). Note that we do not necessarily need to order signals by placing zeros in

the rear. We only write the signal as Eq. (77) for notational convenience. We now apply polynomial filters on signals

$$\mathbf{s}_1 = h_1(\mathbf{s}) = \sum_i a_i \mathbf{A}^{[i]} \diamond \mathbf{s}, \quad (78)$$

$$\mathbf{s}_2 = h_2(\mathbf{s}) = \mathbf{A}^{[i]} \diamond \mathbf{s}, \quad (79)$$

For a filtered signal  $\mathbf{s}_X \in \mathbb{R}^M \times \mathbb{R}^N$  ( $X = 1, 2$ ), we define a function to map 2-D signals into 1-D by calculated the column-wise mean of  $\mathbf{s}_X$ , i.e.,

$$\bar{\mathbf{s}}_X = \text{mean}_{col}(\mathbf{s}_X) \in \mathbb{R}^{1 \times N}. \quad (80)$$

Next, we can define a function  $M(\cdot)$  on  $\bar{\mathbf{s}}_X$  and consider certain objective functions in filter design.

To validate the efficacy of polynomial filtering in the MLN framework, we test  $h_1(\cdot)$  and  $h_2(\cdot)$  for the binary classification problem on the Cleveland Heart Disease Dataset (<https://archive.ics.uci.edu/ml/datasets/heart+disease>). In this dataset, there are 297 data points with 13 feature dimensions. We directly build a MLN with  $N = 297$  nodes in each of the  $M = 13$  layers. More specifically, we directly use the labels in the confidence matrix  $\mathbf{s}$ .

- For  $h_1(\cdot)$  (AF), we set  $a_i \neq 0$  for at least one  $i > 0$ . Using MSE as objective function, we apply a greedy algorithm to estimate parameters  $\{a_i\}$ . We limit the highest polynomial order to 10.
- For  $h_2(\cdot)$  (APF), we estimate a classification threshold based on the mean of  $\bar{\mathbf{s}}_X$  by setting the polynomial order  $i$  to 10.

We compare our methods with GSP-based method in similar setups as in aforementioned examples. The only difference is that we use  $\bar{\mathbf{s}}_X$  in M-GSP and use  $\mathbf{s}' = f(\begin{bmatrix} \mathbf{s}_L \\ \mathbf{0}_{UL} \end{bmatrix})$  in GSP for mapping and classification. We also present the results of label propagation and SVM for comparison. We randomly split the test and training data for 100 rounds. From the results shown in Fig. 6, GSP-based and M-GSP based methods exhibit better performance than traditional learning algorithms, particularly when the fraction of training samples is small. Generally, M-GSP based methods provide superior performance among all methods owing to its power in extracting ‘multilayer’ features.

#### D. Data Compression

Data compression through sampling may efficiently reduce dataset size. Moreover, projecting signals into a suitable manifold or space, one may reveal a sparse representation of the data [45]. In M-GSP, we can also select a subset of transformed signal samples in spectrum domain to approximate the entire signal as suggested in Algorithm 3. Moreover, we can also integrate data encoding to further compress the data size. In this application example, we mainly focus on sampling to test the use of MLN spectrum space to represent structured data.

We test MLN sampling on the RGB icon dataset [12]. This dataset contains several icon images of size  $\mathbb{R}^{16 \times 16}$ . Our goal is to sample a subset of  $K = 16 \times 16 \times 3 = 768$  transformed data points in spectrum domain. We follow Algorithm 3 to sample the transformed data before using the sampled data to recover the original images. In this application, we construct

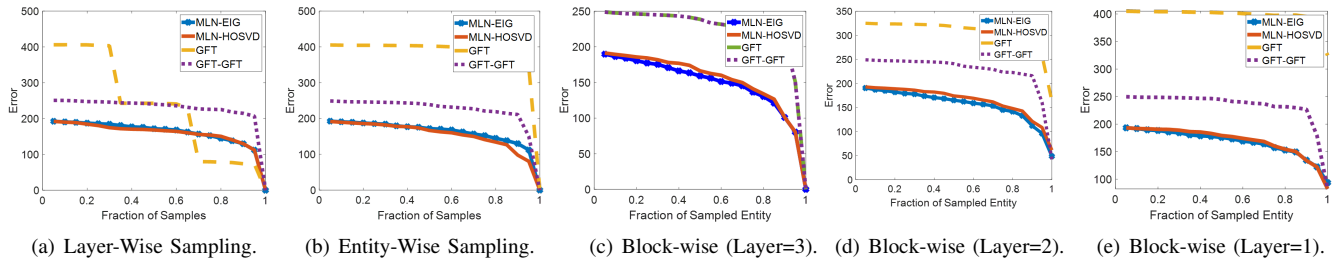


Fig. 7. Results of Sampling in the Order of Frequency.

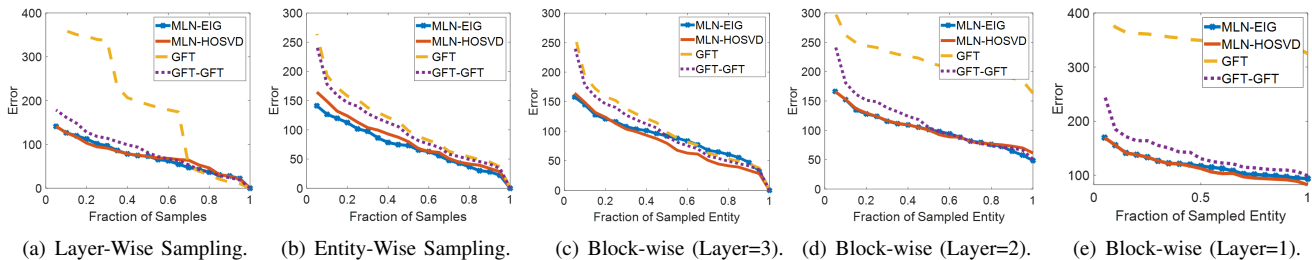


Fig. 8. Results of Sampling in the Order of Transformed Value.

the MLN as described in Section IV-B. We compare our methods with two GSP-based methods.

In the first method (GFT), we build a graph with  $16 \times 16$  nodes and implement GFT on signals in each layer separately. In the second method (GFT<sup>2</sup>), we build a graph of size  $16 \times 16$  for pixels that are neighbor-4 connected (as described in Section IV-B) and construct a graph of size 3 for (fully connected) frames. Let  $\mathbf{E}$  be the spectrum of frame-wise graph, and  $\mathbf{F}$  be the spectrum of pixel-wise graph. We then apply GFT on the 2-D signal  $\mathbf{s} \in \mathbb{R}^3 \times \mathbb{R}^{256}$  to generate  $\hat{\mathbf{s}} = \mathbf{E}\mathbf{s}\mathbf{F}^T$ . For both GSP and M-GSP methods, we apply the Laplacian matrix/tensor. We order the transformed signal in descending order of either the eigenvalues or the transformed values from top left to bottom right, i.e., preserving the low-frequency part in Fig. 7 and keeping larger values in Fig. 8.

As mentioned in Section III-E, there are three directions of sampling node values. In layer-wise sampling, we remove samples layer-by-layer from bottom up. More specifically, we remove samples from right to left when sampling each layer. Similarly, in entity-wise sampling, we remove samples column wise from right to left. When sampling each column, we move from bottom up. In block-wise sampling, we preserve samples in top-left blocks. Since there are only three layers, we present all results of block-wise sampling layer-by-layer in Fig. 7(c)-7(e) and Fig. 8(c)-8(e). Defining *sampling fraction* as the ratio of saved samples to total original signal samples, we measure errors between the recovered and original images. The results from 5% – 100% sampling fraction are shown in Fig. 7 and Fig. 8. These results confirm that the proposed MLN methods provide better performance than GSP.

More specifically, from Fig. 7 where sampling is based on the order of frequency, the MLN singular space shows more efficient representation than MLN eigenspace in layer-wise and entity-wise sampling. This can be attributed to the fact that

M-GST focuses more on separate layer features as discussed in Part I [7]. Additionally, M-GFT is better than M-GST in block-wise sampling, as seen from Fig. 7(a), which indicates the MLN eigenspace could capture the joint data information more efficiently.

When signals are sampled without consider the frequency order, Fig. 8 shows different results. In fact, both MLN-HOSVD and MLN-Eig show similar performances. Generally, different datasets may contain different features in spectral domain, which cause different results from different sampling orders among the methods of Fig. 8. With some prior signal knowledge such as spectrum concentration in terms of signal energy, one could conceivably select a suitable order to implement sampling based on signal properties and sampling objectives.

### E. Other Applications

Through various examples presented so far, we have demonstrated the power of M-GSP in general signal/data processing applications. We also view the multilayer network as useful model for datasets involving spatial temporal features in applications such as robotics and cyber-physical systems. Video processing is also a natural application area. Another application example of motion detection in point cloud sequences has been considered in Part I [7]. We shall continue to M-GSP in a variety of signal processing and data analysis applications in future works.

## V. CONCLUSIONS

Continuing from the introduction and foundation of multilayer network presented in Part I [7], Part II focuses on algorithms, implementation, and application aspects of the M-GSP framework. We develop several useful data processing and analysis tools based on MLN. We provide detailed

discussions on sampling theory, filter design, convolution, and stationary process. Furthermore, we establish multilayer network as an efficient model for processing complex datasets. Through an array of application examples of M-GSP in signal processing and data analysis, we demonstrate the benefits and the practicality of the proposed M-GSP framework.

## REFERENCES

- [1] A. Sandryhaila, and J. M. F. Moura, "Discrete signal processing on graphs" *IEEE Transactions on Signal Processing*, vol. 61, no. 7, pp. 1644-1656, Apr. 2013.
- [2] A. Ortega, P. Frossard, J. Kovačević, J. M. F. Moura and P. Vandergheynst, "Graph signal processing: overview, challenges, and applications," in *Proceedings of the IEEE*, vol. 106, no. 5, pp. 808-828, May 2018.
- [3] M. De Domenico, A. Sole-Ribalta, E. Cozzo, M. Kivela, Y. Moreno, M. A. Porter, S. Gomez, and A. Arenas, "Mathematical formulation of multilayer networks," in *Physical Review X*, vol. 3, no. 4, p. 041022, Dec. 2013.
- [4] M. Kivela, A. Arenas, M. Barthelemy, J. P. Gleeson, Y. Moreno, and M. A. Porter, "Multilayer networks," in *Journal of complex networks*, vol. 2, no. 3, pp. 203-271, Jul. 2014.
- [5] Boccaletti, G. Bianconi, R. Criado, C. I. Del Genio, J. Gomez- Gardenes, M. Romance, I. Sendina-Nadal, Z. Wang, and M. Zanin, "The structure and dynamics of multilayer networks," *Physics Reports*, vol. 544, no. 1, pp. 1-122, Nov. 2014.
- [6] S. Zhang, H. Zhang, H. Li and S. Cui, "Tensor-based spectral analysis of cascading failures over multilayer complex systems," in *Proceedings of 56th Annual Allerton Conference on Communication, Control, and Computing (Allerton)*, Monticello, USA, Oct. 2018, pp. 997-1004.
- [7] S. Zhang, Q. Deng and Z. Ding, "Graph signal processing over multilayer networks – part i: theoretical foundations and frequency analysis." Supplements.
- [8] T. G. Kolda and B. W. Bader, "Tensor decompositions and applications," *SIAM Review*, vol. 51, no. 3, pp. 455-500, Aug. 2009.
- [9] L. De Lathauwer, B. De Moor, and J. Vandewalle, "A multilinear singular value decomposition," *SIAM Journal on Matrix Analysis and Applications*, vol. 21, no. 4, pp. 1253-1278, Jan. 2000.
- [10] A. Sandryhaila, and J. M. F. Moura, "Discrete signal processing on graphs: graph filters," in *Proceedings of 2013 IEEE International Conference on Acoustics, Speech and Signal Processing*, Vancouver, Canada, May 2013, pp. 6163-6166.
- [11] S. Chen, A. Sandryhaila, J. M. F. Moura and J. Kovačević, "Adaptive graph filtering: multiresolution classification on graphs," *2013 IEEE Global Conference on Signal and Information Processing*, Austin, TX, USA, Dec. 2013, pp. 427-430.
- [12] S. Zhang, Z. Ding and S. Cui, "Introducing hypergraph signal processing: theoretical foundation and practical applications," in *IEEE Internet of Things Journal*, vol. 7, no. 1, pp. 639-660, Jan. 2020.
- [13] S. Chen, F. Cerda, P. Rizzo, J. Bielak, J. H. Garrett and J. Kovačević, "Semi-supervised multiresolution classification using adaptive graph filtering with application to indirect bridge structural health monitoring," in *IEEE Transactions on Signal Processing*, vol. 62, no. 11, pp. 2879-2893, Jun. 2014.
- [14] S. Chen, A. Sandryhaila, J. M. F. Moura and J. Kovacevic, "Signal denoising on graphs via graph filtering," *2014 IEEE Global Conference on Signal and Information Processing (GlobalSIP)*, Atlanta, GA, USA, Dec. 2014, pp. 872-876.
- [15] S. Zhang, S. Cui and Z. Ding, "Hypergraph spectral analysis and processing in 3d point cloud," in *IEEE Transactions on Image Processing*, vol. 30, pp. 1193-1206, Dec. 2021.
- [16] K. Avrachenkov, A. Mishenin, P. Gonçalves, and M. Sokol, "Generalized optimization framework for graph-based semi-supervised learning," in *Proceedings of the 2012 SIAM International Conference on Data Mining*, Anaheim, CA, USA, Apr. 2012, pp. 966-974.
- [17] J. Kunegis, S. Schmidt, A. Lommatzsch, J. Lerner, E. W. De Luca, and S. Albayrak, "Spectral analysis of signed graphs for clustering, prediction and visualization," in *Proceedings of the 2010 SIAM International Conference on Data Mining*, Columbus, OH, USA Apr. 2010, pp. 559-570.
- [18] D. Zhou, J. Huang, and B. Schölkopf, "Learning with hypergraphs: clustering, classification, and embedding," *Advances in Neural Information Processing Systems*, Vancouver, Canada, Dec. 2006, pp. 1601-1608.
- [19] S. Zhang, S. Cui and Z. Ding, "Hypergraph-based image processing," *2020 IEEE International Conference on Image Processing (ICIP)*, Abu Dhabi, United Arab Emirates, Oct. 2020, pp. 216-220.
- [20] T. N. Kipf and M. Welling, "Semi-supervised classification with graph convolutional networks," *ICLR*, Toulon, France, Apr. 2017.
- [21] D. I. Shuman, S. K. Narang, P. Frossard, A. Ortega and P. Vandergheynst, "The emerging field of signal processing on graphs: Extending high-dimensional data analysis to networks and other irregular domains," in *IEEE Signal Processing Magazine*, vol. 30, no. 3, pp. 83-98, May 2013.
- [22] J. Shi, and J. M. Moura, "Graph signal processing: Dodulation, convolution, and sampling," arXiv:1912.06762, 2019.
- [23] A. G. Marques, S. Segarra, G. Leus, and A. Ribeiro, "Stationary graph processes and spectral estimation," *IEEE Transactions on Signal Processing*, vol. 65, no. 22, pp. 5911-5926, Aug. 2017.
- [24] G. Mateos, S. Segarra, A. G. Marques, and A. Ribeiro, "Connecting the dots: Identifying network structure via graph signal processing," *IEEE Signal Processing Magazine*, vol. 36, no. 3, pp. 16-43, May 2019.
- [25] B. Pasdeloup, V. Gripon, G. Mercier, D. Pastor, and M. G. Rabbat, "Characterization and inference of graph diffusion processes from observations of stationary signals," *IEEE Transactions on Signal and Information Processing over Networks*, vol. 4, no. 3, pp. 481-496, Aug. 2017.
- [26] K. I. Park, *Fundamentals of probability and stochastic processes with applications to communications*. Springer International Publishing, 2018.
- [27] S. Segarra, A. G. Marques, G. Mateos, and A. Ribeiro, "Network topology inference from spectral templates," *IEEE Transactions on Signal and Information Processing over Networks*, vol. 3, no. 3, pp. 467-483, Sep. 2017.
- [28] X. Dong, D. Thanou, P. Frossard, and P. Vandergheynst, "Learning Laplacian matrix in smooth graph signal representations," *IEEE Transactions on Signal Processing*, vol. 64, no. 23, pp. 6160-6173, Dec. 2016.
- [29] X. Dong, D. Thanou, M. Rabbat, and P. Frossard, "Learning graphs from data: a signal representation perspective," *IEEE Signal Processing Magazine*, vol.36, no. 3, pp. 44-63, Apr. 2019.
- [30] S. Zhang, S. Cui and Z. Ding, "Hypergraph spectral clustering for point cloud segmentation," in *IEEE Signal Processing Letters*, vol. 27, pp. 1655-1659, Sep. 2020.
- [31] M. N. Marshall, "Sampling for qualitative research," *Family Practice*, vol. 13, no. 6, pp. 522-526, Dec. 1996.
- [32] S. Chen, R. Varma, A. Sandryhaila and J. Kovačević, "Discrete Signal Processing on Graphs: Sampling Theory," in *IEEE Transactions on Signal Processing*, vol. 63, no. 24, pp. 6510-6523, Dec.15, 2015.
- [33] P. Lorenzo, S. Barbarossa, and P. Banelli, "Sampling and recovery of graph signals," in *Cooperative and Graph Signal Processing*, pp. 261-282, 2018.
- [34] A. Gadde, and A. Ortega, A. "A probabilistic interpretation of sampling theory of graph signals," in *2015 IEEE International Conference on Acoustics, Speech and Signal Processing (ICASSP)*, Brisbane, Australia, Apr. 2015, pp. 3257-3261.
- [35] W. Kim, A. Kanazaki and M. Tanaka, "Unsupervised learning of image segmentation based on differentiable feature clustering," in *IEEE Transactions on Image Processing*, vol. 29, pp. 8055-8068, Jul. 2020.
- [36] U. Von Luxburg, "A tutorial on spectral clustering," *Statistics and Computing*, Vol. 17, no. 4, pp. 395-416, Aug. 2007.
- [37] K. Wagstaff, C. Cardie, S. Rogers, and S. Schroedl, "Constrained k-means clustering with background knowledge," in *ICML*, Williamstown, MA, USA, Jun. 2001, pp. 577-584.
- [38] D. Martin, C. Fowlkes, D. Tal and J. Malik, "A database of human segmented natural images and its application to evaluating segmentation algorithms and measuring ecological statistics," *Proceedings Eighth IEEE International Conference on Computer Vision*, Vancouver, BC, Canada, Jul. 2001, pp. 416-423.
- [39] X. Ji, J. F. Henriques, and A. Vedaldi, "Invariant information clustering for unsupervised image classification and segmentation," in *Proceedings of the IEEE International Conference on Computer Vision*, Seoul, Korea, Nov. 2019, pp. 9865- 9874.
- [40] P. F. Felzenszwalb and D. P. Huttenlocher, "Efficient graph-based image segmentation," *International Journal of Computer Vision*, vol. 59, no. 2, pp. 167-181, 2004.
- [41] A. Kanazaki, "Unsupervised image segmentation by backpropagation," in *Proceedings of IEEE International Conference on Acoustics, Speech, and Signal Processing (ICASSP)*, Calgary, AB, Canada, Apr. 2018, pp. 1543-1547.
- [42] A. K. Cherri, and M. A. Karim, "Optical symbolic substitution: edge detection using Prewitt, Sobel, and Roberts operators," *Applied Optics*, vol. 28, no. 21, pp. 4644-4648, Nov. 1989.
- [43] L. Ding, and A. Goshtasby, "On the Canny edge detector," *Pattern Recognition*, vol. 34, no. 3, pp. 721-725, Mar. 2001.
- [44] X. Zhu, and Z. Ghahramani, "Learning from labeled and unlabeled data with label propagation," *CMU CALD Tech Report*, vol. 02, no. 107, 2002.

- [45] A. Sandryhaila and J. M. F. Moura, "Discrete signal processing on graphs: frequency analysis," in *IEEE Transactions on Signal Processing*, vol. 62, no. 12, pp. 3042-3054, Jun., 2014.